Astrophysical tests of modified gravity: Stellar and gaseous rotation curves in dwarf galaxies

Vinu Vikram,[1,2,*] Jeremy Sakstein,[2,3,4,†] Charles Davis,[2] and Andrew Neil[2]

[1]*Argonne National Laboratory, 9700 South Cass Avenue, Lemont, Illinois 60439, USA*
[2]*Center for Particle Cosmology, Department of Physics and Astronomy, University of Pennsylvania, 209 S. 33rd Street, Philadelphia, Pennsylvania 19104, USA*
[3]*DAMTP, Centre for Mathematical Sciences, University of Cambridge, Wilberforce Road, Cambridge CB3 0WA, United Kingdom*
[4]*Perimeter Institute for Theoretical Physics, 31 Caroline Street North, Waterloo, Ontario N2L 6B9, Canada*

(Received 14 February 2018; published 30 May 2018)

Chameleon theories of gravity predict that the gaseous component of isolated dwarf galaxies rotates with a faster velocity than the stellar component. In this paper, we exploit this effect to obtain new constraints on the model parameters using the measured rotation curves of six low surface brightness galaxies. For $f(R)$ theories, we rule out values of $f_{R0} > 10^{-6}$. For more general theories, we find that the constraints from Cepheid variable stars are currently more competitive than the bounds we obtain here but we are able to rule out self-screening parameters $\chi_c > 10^{-6}$ for fifth-force strengths (coupling of the scalar to matter) as low as 0.05 the Newtonian force. This region of parameter space has hitherto been inaccessible to astrophysical probes. We discuss the future prospects for improving these bounds.

DOI: 10.1103/PhysRevD.97.104055

I. INTRODUCTION

Infrared modifications of general relativity (GR) have received attention recently as possible candidates to explain the acceleration of the Universe (see [1–4] and references therein for a review). Among the plethora of proposed theories, those that include screening mechanisms—which give rise to novel features on cosmological scales but hide any modifications of general relativity in our own solar system—are particularly well studied due to their ability to satisfy local tests of general relativity without the need for fine-tuning. These fall into two categories: the Vainshtein mechanism [5]—which screens by suppressing scalar field gradients—and those that screen by suppressing the scalar charge to mass ratio, which include the chameleon effect [6,7], the symmetron mechanism [8], and the environment-dependent Damour-Polyakov effect [9]. This paper is concerned with the latter class.

Recently, several authors [10–27] have shown that astrophysical tests have the potential to probe parameter ranges inaccessible to laboratory experiments or cosmological probes (for a review of these tests see [3,4,12,28–30]). These tests include the structure and evolution of stars, kinematical and morphological studies of dwarf galaxies, discrepancies between the dynamical and lensing masses of galaxy clusters, and the offset between compact objects and stellar components in dwarf galaxies. In the first of a series of papers, [31] compiled a screening map of the nearby universe, which identified which galaxies are unscreened as a function of the model parameters. This was the first step towards making these (at the time) theoretical tests possible. In the second paper, [15] compared the observed Cepheid and tip of the red giant branch distances to unscreened galaxies in the map and were able to place the strongest constraints to date. In the third paper [17] attempted to perform the tests using the morphology and kinematics of the galaxies in the map but were unable to place further constraints. This paper, the fourth in the series, is concerned with the final observational signature that has not yet been tested observationally.

As mentioned above, chameleonlike theories screen by suppressing the scalar charge of an object relative to its mass and [13] have used this feature to suggest a novel signature. Stars, being compact objects, are screened and hence have zero scalar charge. This means their motion in modified theories of gravity is identical to that predicted by general relativity. Conversely, diffuse gas is unscreened and feels the full fifth-force present due to the modifications. This means that at fixed radius, the gaseous component of an unscreened galaxy should rotate with a higher velocity than the stellar component. [13] estimate that this difference can be as high as 10–15 km/s depending on the galaxy's mass and the model parameters.

*vvinuv@gmail.com
†sakstein@physics.upenn.edu

Reference [17] investigated the possibility of carrying out this test using currently available data, but they were unable to test the difference between the stellar and gaseous rotation curves. The main reason for this is the following: Historically, the rotation curves of galaxies are measured using either Hα or the 21 cm line. Hα is produced by the recombination of hot ionized gas around massive stars, called the Stromgren sphere, whilst the 21 cm line is produced by neutral hydrogen gas. Both of these lines probe the unscreened gaseous components of the galaxies. Hence, there is no screened component with which to compare the measured rotation velocities and no quantitative statements could be made. This leaves the effect described above an untested prediction.

With high quality data, it would be possible to derive the stellar rotation curves from stellar absorption lines. In this paper we do this using data obtained for six low surface brightness galaxies by [32] and attempt to constrain the model parameters. One well-studied theory which utilizes the chameleon effect is $f(R)$ gravity [33]. The general class of chameleonlike theories is parametrized by two numbers but $f(R)$ theories have one of these fixed, which makes them useful prototype theories to explore. These theories are parametrized by the dimensionless number f_{R0}. More general chameleon (and similar) models have two parameters, χ_c and α.

This paper is organized as follows: In Sec. II, we give a brief introduction to chameleon theories of gravity and describe the observational effect we are looking for. In Sec. III, we describe the data we will use and briefly summarize the measurement of stellar and gaseous rotation curves. Section IV describes the systematics involved in the measurement and possible ways to correct it, and Sec. V describes the analysis of the rotation curves. We discuss our results and draw our conclusions in Secs. VI and VII, respectively.

II. CHAMELEON SCREENING AND $f(R)$ GRAVITY

In this section, we will briefly describe the screening mechanism and elucidate the model parameters. Chameleon models include a new scalar degree of freedom that couples to matter, giving rise to an additional gravitational strength force. Laboratory searches for fifth-forces would generally constrain such theories to levels at which they become uninteresting but the chameleon mechanism acts to suppress the fifth-force locally, thereby evading them. This is achieved by arranging the field equations such that the scalar's mass in high-density environments is larger than the inverse micron scales probed by current experiments. These experiments, therefore, leave a large region of parameter space unconstrained. On larger—inter-galactic and cosmological—scales, the mass can be far smaller and $\mathcal{O}(1)$ fifth-forces can give rise to new and novel effects.

On small (astrophysical) scales, and when any relevant time-scale is small compared to the Hubble time, the entire class of chameleon models can be parametrized by two dimensionless parameters α and χ_c. Any over-dense spherical object of radius R embedded into a larger, underdense medium will be characterized by a screening radius r_s, which is not an independent parameter, but is determined by χ_c in a manner to be made precise below. In the region interior to the screening radius, there is no fifth-force, and the total force is the Newtonian one. Exterior to this region, the total force is given by

$$F(r > r_s) = \frac{GM(r)}{r^2}\left[1 + \alpha\left(1 - \frac{M(r_s)}{M(r)}\right)\right] \quad r > r_s, \quad (1)$$

where $M(r)$ is the mass enclosed by radius r. Note that when $r_s = R$ the object is fully screened and the force is simply the Newtonian one, whereas when $r_s = 0$ the object is fully unscreened and the strength of gravity is enhanced by a factor of $(1 + \alpha)$. α then parametrizes the strength of the chameleon force and is identically equal to $1/3$ in $f(R)$ models [33]. The self-screening parameter χ_c determines how efficient an object is at screening itself.[1] as a rule of thumb, if χ_c is smaller than the surface Newtonian potential GM/Rc^2 the object is screened. If the converse is true, the object will be partially unscreened. Very roughly, $\chi_c \sim H_0^2\lambda_C^2/c^2$ where λ_C is the Compton wavelength of the field in the cosmological background. In $f(R)$ theories, one has $\chi_c = 3/2f_{R0}$ [34] and therefore, have only one free parameter. Currently, the strongest constraint on f_{R0} was obtained by [15] who find $f_{R0} \lesssim 3 \times 10^{-7}$. Importantly, χ_c (or f_{R0} for $f(R)$ theories) determines the screening radius through the implicit relation

$$\int_{r_s}^{\infty} r\rho(r)dr = \frac{\chi_c c^2}{4\pi G}. \quad (2)$$

If this has no solution, then $r_s = 0$ and the object is unscreened. The derivation of this formula can be found in [10,14,18] but here we remark that the only approximation used to obtain it is that the mass of the field is negligible compared with the inverse length scale in question. This is completely consistent with the approximation used to obtain Eq. (1) and is known to hold well inside stars and galaxies.[2] Going beyond this approximation introduces a high degree of model-dependency and yields only small corrections to the final results. In what follows, we will use Eq. (2) to determine the screening radius of each galaxy in our sample assuming realistic density profiles to be specified below.

[1]Self-screening here refers to the fact that object may be screened by the presence of massive neighbors. See [10] for a discussion of this.

[2]See [14,18,35] for a more detailed discussion on this.

III. DATA AND REDUCTION

In this work, we will use the rotation curves of six low surface brightness galaxies measured by [32]. They derived the rotation curves using both absorption and emission lines, which probe the rotation velocities of stars and gaseous components, respectively. Rotation curves are generated using data collected from the ESO Very Large Telescope (VLT)-FORS2 instrument. The spectroscopic wavelength range of the spectra is between 4750 and 5800 Å. This range includes useful stellar absorption lines, such as the Mgb triplet, and emission lines, such as Hβ and [OIII]. The rotation curve for the gaseous component was obtained by fitting Gaussians to these emission lines simultaneously. In addition to the spectroscopic data, they acquired deep, high resolution photometric data for these galaxies. This was done using Gunn-z filter, which probes the older stellar populations in the galaxy. Photometric data help to identify the morphologies and generate structure parameters for these galaxies. In Table I, we show a few relevant properties of these galaxies.

A. Screening level of galaxies

It is essential for our test to know the screening level of a galaxy given a set of model parameters. We check the screening level of a galaxy based on the procedure described in [31]. The screening map classifies the galaxies as either screened or unscreened based on two proxies that estimate whether they are self-screened due to their own Newtonian potential or environmentally screened due to the potential of their neighbors. In the former case, the criterion for self-screening is well understood: galaxies will be unscreened when the self-Newtonian potential $\Phi_{\rm N}^{\rm self} = GM/r_{\rm vir}c^2$—$r_{\rm vir}$ is the virial radius—is smaller than $\chi_c(=3/2f_{R0})$. This is estimated on a galaxy by galaxy basis using the relation $GM/r_{\rm vir} = v_{\rm c}^2$ where $v_{\rm c}$ is the peak circular velocity. The criterion for environmental screening is not so clear and there has been an intense effort in the N-body community aimed at finding reliable proxies for environmental screening [37,38]. The screening map uses the approximation that the level of environmental screening is set by the external Newtonian potential,

$$\Phi_{\rm N}^{\rm ext} = \sum_{d<\lambda_{\rm C}+r_i} \frac{GM_i}{r_i}, \tag{3}$$

where d_i is the distance to the galaxy with mass M_i and virial radius r_i. The sum extends over galaxies inside the Compton wavelength ($\lambda_{\rm C} = 1, 3, 10$ Mpc for $f_{R0} = 10^{-7}, 10^{-6}, 10^{-5}$). The motivation behind this is that the chameleon force is suppressed outside the Compton wavelength so that the fields sourced by any galaxies outside a sphere of radius $\lambda_{\rm C}$ will have attained their asymptotic values.

Based on the data described in [31], we estimate the Newtonian potential due to environment for all the six galaxies in our sample. It is found that, with the exception of galaxy ESO 2340130, all other galaxies inhabit regions where the Newtonian potentials is low enough that they are not environmentally screened. Therefore, it is possible to test chameleon theories if their self-Newtonian potential is less than the given value of χ_c. In Table I, we show the values of the Newtonian potential due to environment for different f_{R0} values.

We derive the self-Newtonian potential of the galaxies using their stellar rotation curve. We are interested in probing $\chi_c < 10^{-6}$. At these low values, main-sequence stars are screened and hence have zero scalar charge. Therefore, they move according to general relativity and their rotation velocity traces the true mass of the galaxy.[3] Also, we assume that the galactic density profile is described by either an NFW or core-singular isothermal sphere (cSIS) model [39],

$$\rho(r) = \frac{\rho_0}{(r/r_0)(1+(r/r_0)^2)} \qquad \text{NFW} \tag{4}$$

$$\rho(r) = \frac{\rho_0}{1+(r/r_0)^2} \qquad \text{cSIS}, \tag{5}$$

where ρ_0 and r_0 are the central densities and scale radii, respectively. When determining the screening level of a specific galaxy, we will use the empirically fitted profiles in conjunction with Eq. (2) to find the screening radius. The ∞ in the upper limit is really a proxy for the radius at which the field reaches its cosmic value. The NFW profile [Eq. (4)] falls off sufficiently quickly at large radii that this may be performed exactly but the cSIS profile [Eq. (5)] has a slower falloff and is unphysical at large radii. For this reason, we integrate to R_{200} in order to determine the screening radius. One should really integrate to a few Compton wavelengths out from this; however, this will introduce some model dependency. Integrating to R_{200} is

TABLE I. Basic parameters of galaxies in our sample. (1) D: Distance to the galaxy (Mpc); (2) i: inclination angle; (3) B/T: bulge to total ratio from [32]; (4) ϕ_1, ϕ_2, ϕ_3: Newtonian potential of the environment for Compton scales of 1, 2, and 3 Mpc which corresponds to $f_{R0} \sim 1\times10^{-7}$, $f_{R0} \sim 4\times10^{-7}$ and $f_{R0} \sim 1\times10^{-6}$, respectively [36].

Galaxy	D	i	B/T	ϕ_1	ϕ_2	ϕ_3
ESO 4880490	37.5	67	0.21	0	0	0
ESO 2060140	60.5	39	0.04	0	0	0
ESO 2340130	60.9	69	0.66	1.3×10^{-6}	1.3×10^{-6}	1.3×10^{-6}
ESO 4000370	60.1	50	0.03	0	0	0
ESO 1860550	25	63	0.68	7.6×10^{-8}	7.6×10^{-8}	1.7×10^{-7}
ESO 5340200	226.7	46	0.56	0	0	0

[3] In this context, the true mass of the galaxy is identical to its lensing mass.

completely consistent with the approximation that the mass is negligible, and we have checked that the results are robust to changing the upper limits to a few times R_{200}.

It should be noted that the dominant dark matter component of the galaxy could be unscreened so that it may deviate from the standard NFW or cSIS profiles [40]. We do not consider this effect in this study. We fit the stellar rotation curve to derive the scale radii and central densities of for each profile. These fitted parameters are then used to estimate the Newtonian potential of the galaxies. Based on the uncertainties in the fitted parameters, we found that cSIS gives a better fit to all of the rotation curves except for ESO 5340200. In Table II, we show the fitted parameters for the cSIS and NFW models. Based on the environmental and self-Newtonian potentials, we estimate the value of f_{R0} above which each galaxy becomes unscreened. This implies that each galaxy allows us to probe different values of f_{R0}. These values are also shown in Table II.

Finally, we note that there may be uncertainties in the environmental screening level due to *missing mass* [41,42]. In particular, N-body simulations have shown that density perturbations on scales smaller than ∼10 Mpc could be enhanced by factors of 50–100% due to dark matter that does not include any visible host galaxies or that hosts galaxies too faint to be resolved in the 2M++ survey. These would still contribute to the environmental value of the Newtonian potential and could potentially enhance the screening level by 5–10%. Unfortunately, missing mass is not accounted for in the screening map of [31] so we are unable to estimate its effects on our galaxies. One could reduce the uncertainty associated with missing mass using forward Bayesian modeling applied to large sample sizes as was done recently by reference [43].

B. Spectral lines used in the analysis

It is important to be sure that we are probing both the screened and unscreened components. This is achieved by our choice of absorption and emission lines. The Mg*b* triplet lines are due to absorption in the atmospheres of G- and K-type stars [44]. These are low mass (0.6–$1.2M_\odot$) main-sequence stars with temperatures between 4000 and 7000 K. These stars have Newtonian potentials $\Phi_N \sim \mathcal{O}(10^{-6})$ and are hence self-screened when $\chi_c \lesssim 10^{-6}$. We can therefore use the rotation curve measured using these lines as a tracer of the screened component of the galaxy. The three absorption lines used by [32] have wavelengths 5164, 5173 and 5184 Å. It should be noted that giant stars can also contribute to the Mg*b* absorption lines but this is small enough to ignore in this study [45]. On the other hand, [OIII] emission lines result from forbidden transitions from doubly ionized oxygen in a metastable state. This line only exists at extremely low densities. At higher densities, inelastic collisions relax the system to a stable state without the emission of photon. These lines therefore probe the unscreened gaseous component of the galaxies.

Before going further, it is instructive to pause and comment on the range of χ_c that can be probed with our rotation curve analysis. As remarked above, the main-sequence stars used to calculate the stellar rotation curve have Newtonian potentials of order 10^{-6} and are hence unscreened when $\chi_c \gtrsim 5 \times 10^{-6}$. When this is the case, the stars probed by the Mg*b* absorption lines rotate at the same speed as the gaseous component and there is no offset between the two components. Therefore, the offset of the two rotation curves probes only a narrow range in χ_c. The lower limit is set by the Newtonian potential of the galaxy and/or the environment (typically $\mathcal{O}(10^{-8})$–$\mathcal{O}(10^{-7})$ for the galaxies in our sample) and the upper limit is set by the value of χ_c above which G- and K-type stars unscreened.[4]

TABLE II. The best fit cSIS and NFW parameters for the stellar rotation curves. Columns: ρ_0 and r_0 are defined as in Eqs. (4) and (5). These have unit $M_\odot$ pc^{-3} and parsec. f_{R0} is the value above which the galaxy is completely unscreened.

	cSIS		
Galaxy	r_0	ρ_0	f_{R0}
ESO 4880490	2.0×10^3	4.0×10^{-2}	2.34×10^{-7}
ESO 2060140	3.1×10^3	5.1×10^{-2}	7.39×10^{-7}
ESO 2340130	1.1×10^3	3.9×10^{-1}	9.04×10^{-7}
ESO 4000370	7.2×10^3	3.7×10^{-2}	2.77×10^{-6}
ESO 1860550	1.5×10^3	3.5×10^{-1}	1.49×10^{-6}
	NFW		
Galaxy	r_0	ρ_0	f_{R0}
ESO 5340200	3.4×10^3	4.2×10^{-1}	1.94×10^{-6}

IV. SYSTEMATIC CORRECTIONS TO THE ROTATION CURVES

It is important to understand different systematic uncertainties associated with rotation curves based on stellar absorption lines and gaseous emission lines. In this section, we describe the two major systematics in the rotation curve estimates which could possibly mimic a modified gravity signal. Gaseous rotation curves are known to be affected by noncircular motions. This could be due to the presence of star forming regions and other morphological components such as bars and spiral structures [46]. Based on a sample of 19 galaxies, [47] have shown that the noncircular velocity

[4]In practice, most stars will be unscreened when $\chi_c \gtrsim 5 \times 10^{-6}$. Main-sequence stars obey a well-known mass-radius relation $R \propto M^\nu$, where ν lies in the range 0.2–0.8 depending on the stellar mass. Stars bluer than those probed by the Mg*b* triplet are more massive and hence have smaller Newtonian potentials. Redder stars have $\nu \approx 0.2$ appropriate for the PPI chain and so the Newtonian potential is a very weak function of mass for these stars.

is ≈7 km/s for galaxies with similar magnitudes and rotational velocities to those in our sample. This systematic component in the gaseous rotation curve can potentially mimic a modified gravity signal as it makes the gaseous rotation appear faster than it truly is. In our analysis we subtract the average velocity found by [47] from all the gaseous rotation curves as follows:

$$V^2_{\rm gas,cor} = V^2_{\rm gas,obs} - V^2_{\rm sys} \tag{6}$$

where $V_{\rm gas,obs}$, $V_{\rm gas,cor}$, $V_{\rm sys}$ are the observed, corrected rotation velocities and the noncircular velocity, respectively.

In addition to the above, systematic, asymmetric drift could potentially make the stellar rotation appear slower than the true underlying circular velocity, which could introduce pseudo signal into the data. We attempt to correct the observed rotation velocity based on the observed velocity dispersion and Jeans equations using the following assumptions: According to [48,49], if

(1) the stellar component follows an exponential density profile,
(2) $\sigma^2_\phi/\sigma^2_R \approx 0.5$, where σ_ϕ and σ_R are the velocity dispersions along the azimuthal and radial directions (in cylindrical coordinates), respectively,
(3) $v_z v_R \approx 0$, i.e., the product of the velocities along radial and perpendicular (z direction) to the disk is small and
(4) $\partial \ln \sigma^2_R/\partial \ln R \approx 0$, i.e., the gradient of radial velocity dispersion is small,

then the corrected circular velocity can be written as

$$v^2_c = v^2_\phi + \sigma^2_\phi\left(2\frac{R}{R_{\rm exp}} - 1\right), \tag{7}$$

where $R_{\rm exp}$ is the scale radius of the exponential disk. [32] shows that the galaxies in our sample can be modeled with one or two exponential profiles but three of these galaxies are dominated by the inner exponential bulge component. This is evident from the bulge-to-total light estimated by [32] (see Table I). We exclude the central bulge dominated region of the galaxies from the analysis to reduce any noncircular contamination from bulge. It should be noted that in Eq. (7) we use the average value of the measured velocity dispersion outside the bulge to estimate the correction.

In the latter part of the paper we will see that asymmetric drift correction leads to larger values for stellar rotation curves. This implies that without the asymmetric drift correction, the stellar rotation curve appears systematically lower and can be misidentified as modified gravity signal when compared with the gaseous rotation curve.

V. ANALYSIS OF THE ROTATION CURVES

Once the systematics are accounted for, any difference between the stellar and gaseous rotation velocities is a probe of modified gravity. The stellar and gaseous curves are measured at slightly different radii from the center of the galaxy. Therefore, in order to estimate the difference between them we need to interpolate one or the other to a common radius. Since the gaseous rotation curve is measured at many more finely spaced points than the stellar rotation curve, it is better to interpolate the gaseous rotation curves and leave the stellar curves as measured. Finally, the average values of the gaseous and stellar rotational velocities of both sides of the galaxy is found. It is also possible to take the averages of the rotation curves without interpolation, however this average depends on the locations of the measured points. This means that if there are many measured points in the inner regions, the average can be biased towards a lower rotational velocity.

The gaseous rotation curve can be measured out to larger radii than the stellar curve. Therefore, in order to make a fair comparison with the stellar rotation curve, we need to truncate the gaseous rotation curve at radii larger than the maximum radius where the stellar curve is measured. This ensures that we are comparing the rotation velocities in the same region of the galaxy. In addition to this upper limit on the rotation curve radius, we also need to set a lower limit, which helps to avoid the bulge dominated central region of the galaxy. This means that we consider only those velocity points measured at radii larger than the bulge scale radius R_e. We check whether the final results depend on this choice of radius by repeating the analysis with a range of different lower limits, ranging from $0.5R_e$ to $1.75R_e$. In all cases we find that the final result does not depend on the choice of lower limit, except for the galaxy ESO 1860550. ESO 1860550 shows an increase in the difference between the gaseous and stellar rotation curves between 0.5 and 1.5 times the bulge scale radius. The difference in velocity curves increases from -25 ± 7 km/s at $0.5R_e$ to -60 ± 9 km/s at $1.75R_e$. This galaxy is bulge dominated (B/T = 0.68, see Table I) with a concentrated bulge component (Sersic index $n > 2$) compared with the rest of the galaxies, and therefore this increase may be associated with the large velocity dispersion in the bulge. Later it can be seen that ignoring larger number of observations from the inner part of the rotation curve only strengthen our results.

We give the inverse variance weighted average values of the stellar and gaseous rotation curves in Table IV; we assume that the measured points are uncorrelated. Next to the average value we show the statistical error. In addition to the statistical error, there could be some intrinsic scatter associated with the average rotation velocity. This is due to the fact that the observed rotation curve is not very smooth. This scatter could be introduced by different components such as star forming regions, dust, and other morphological components of the galaxies. We estimate the intrinsic scatter from the residual rotation curve by subtracting the best fit model from the observed rotation curve. This

is done separately for both the stellar and gaseous rotation curves. We quantify the intrinsic errors as follows,

$$\sigma_{\rm int} = \sigma_v/\sqrt{N}, \tag{8}$$

where σ_v is the scatter in the residual rotation velocity curve and N is the number of measured velocity data points. The intrinsic scatter is shown in Table IV after the statistical error. It can be seen that the intrinsic error dominates over the statistical error for most of the galaxies.

One of the most important sources of error in all astrophysical tests of gravity is the uncertainty due to nongravitational astrophysical processes. This means that the difference between the measured stellar and gaseous rotation velocities could be due to astrophysical scatter instead of modified gravity effects. Earlier papers in the series estimated this uncertainty from a sample of screened galaxies and subtracted it statistically from the unscreened sample. We apply the same technique in this paper. The number of objects in the current sample is very small and therefore it is not possible to estimate the astrophysical scatter from a screened sample. We therefore take the scatter in the measured velocity difference of all six galaxies as the astrophysical scatter ($\sigma_{\rm ap}$). In this process we assume that the scatter measured from all galaxies is closer to the underline true value (i.e., the one measured from screened galaxies only) and that the true scatter can be measured from six galaxies. It is possible that the $\sigma_{\rm ap}$ could be overestimated by this process and therefore our conclusions may be conservative. Finally, similar to the earlier papers we assume that $\sigma_{\rm ap}$ scales with the mass of the galaxy. $\sigma^i_{\rm ap}$ of ith galaxy is estimated as

$$\sigma^i_{\rm ap} = \frac{v_i}{N}\sum\frac{\delta_v}{v}, \tag{9}$$

where v_i is the average of the stellar and gaseous velocities of the ith galaxy, δ_v is the uncorrected velocity difference between the gas and stars; the sum runs over all six galaxies. We show $\sigma_{\rm ap}$ in Table IV as the third source of error.

The scatter in Table III is commensurate with the scatter seen in N-body simulations, although it should be noted that observed variations in the rotation curves of dwarf galaxies is typically larger than this [50]. This implies that there may be unknown systematics not accounted for in our astrophysical scatter. Another potential uncertainty is a potential deviation from the NFW profile in the central regions of the galaxy. Dwarf galaxies, being dark matter dominated, are not so susceptible to the effects of baryons at the center and, besides, we exclude the central bulge from our analysis since contributions from the noncircular velocity to the rotation curve may be important there. Nonetheless, the simple NFW profile ignores dark matter substructure, which can contribute as much as 10% of the Halo's mass [51]. This could potentially increase the galaxy's level of self-screening. Finally, high resolution N-body simulations have shown that the halo mass function can be enhanced by up to 20% even in cases where $f_{R0} \sim 10^{-6}$ so one may expect more self-screened galaxies. Our galaxies are selected from the screening map of [31], which uses proxies for the self-screening calibrated on the N-body simulations of [37,38]. This suggests that our classification of galaxies as unscreened is robust to enhancements in the halo mass function, although there may be small uncertainties in the proxies themselves if the density enhancement was not identified in the simulations of [37,38]. A quantitative accounting of these effects is clearly outside the scope of the present work due to the limitations of the screening map but future efforts aimed at constructing more comprehensive maps could elucidate how the features mentioned here impact the screening status of individual galaxies [42].

TABLE III. The measured stellar and gaseous velocities. These values are not corrected for asymmetric drift and noncircular motions.

Galaxy	$v_{\rm gas}$ (km/s)	$v_{\rm star}$ (km/s)
ESO 4880490	$56.56 \pm 2.77 \pm 1.93$	$48.86 \pm 5.37 \pm 6.04$
ESO 2060140	$88.42 \pm 1.65 \pm 3.59$	$65.77 \pm 2.39 \pm 6.54$
ESO 2340130	$114.16 \pm 1.87 \pm 1.69$	$110.75 \pm 2.24 \pm 1.63$
ESO 4000370	$83.51 \pm 2.24 \pm 1.42$	$57.92 \pm 2.99 \pm 7.07$
ESO 1860550	$119.91 \pm 3.57 \pm 5.32$	$137.79 \pm 3.15 \pm 2.69$
ESO 5340200	$272.01 \pm 3.65 \pm 2.82$	$239.45 \pm 4.56 \pm 6.15$

VI. RESULTS AND DISCUSSION

In Tables III and IV, we show the gaseous and stellar rotation velocities before and after systematic corrections along with statistical error, intrinsic and astrophysical scatters in the measurements. Table IV shows the observed difference between the stellar and gaseous velocities and the $f(R)$ prediction. The $f(R)$ prediction is valid for the range of f_{R0} which makes the galaxies unscreened; this is given in Table II. Therefore, $G_{\rm eff} = 4/3G$ is used for all galaxies to get the prediction. Tables III and IV show that the trend found in the observed velocity differences are qualitatively similar for all of the galaxies both before and after the systematic correction. We therefore use the systematic corrected values from here on. The final column in these tables shows the statistical significance (σ) with which we can reject the predicted difference between the gaseous and stellar rotation curves based on the observed value and is defined as

$$\sigma = (\delta_v^{\rm measured} - \delta_v^{\rm predicted})/\text{Measured error}; \tag{10}$$

i.e., $\sigma = 0$ implies that the predicted and measured values agree perfectly and negative (positive) σ imply that stars rotate faster (slower) than the gaseous components. $f(R)$ theories, and, indeed, more general chameleonlike theories

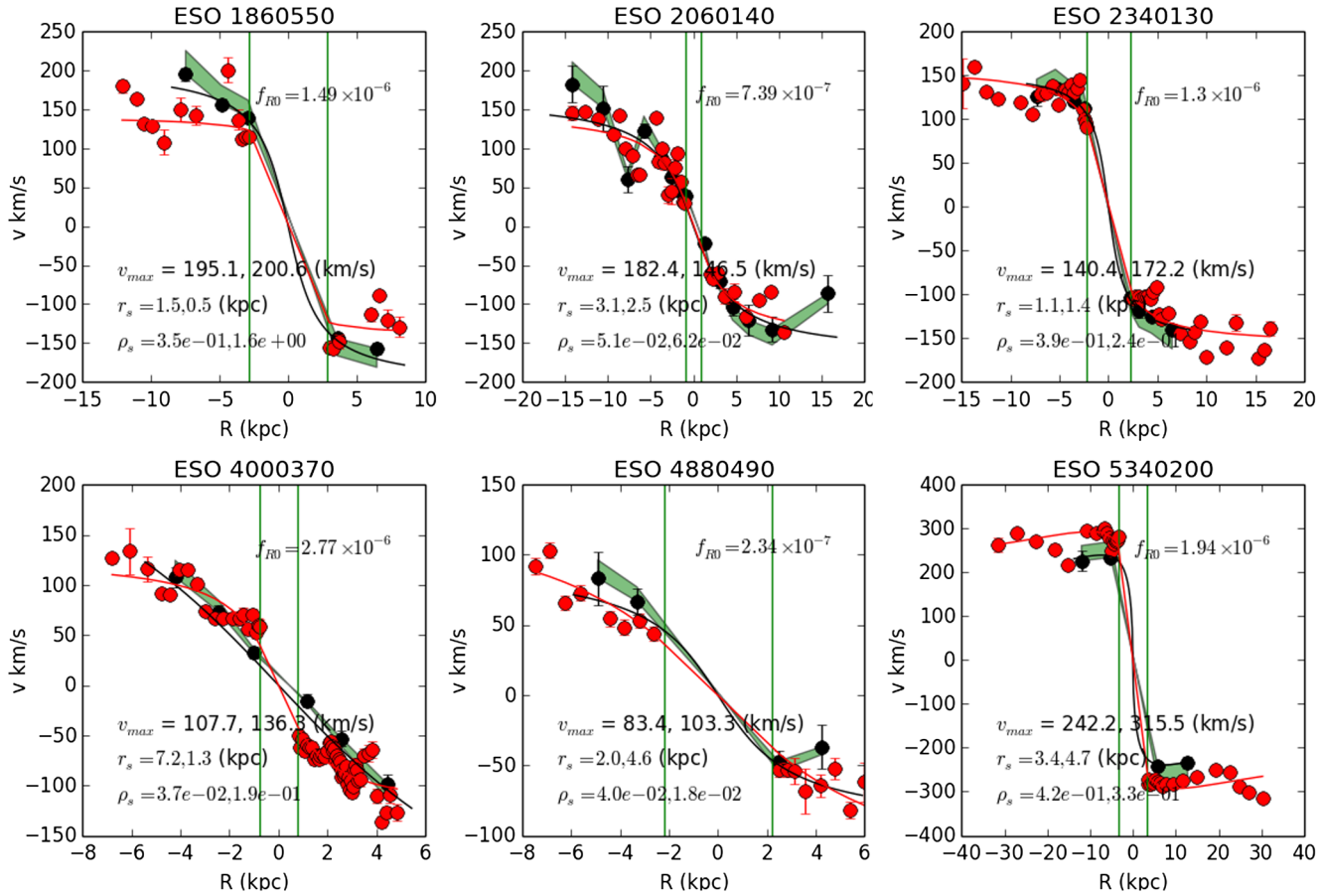

FIG. 1. The rotation curves of the six galaxies in our sample. The black and red points show the stellar and gaseous rotation curves, respectively. The green shaded region shows the $f(R)$ prediction for the rotation velocity of the gaseous component assuming that the galaxy is fully unscreened. The value of f_{R0} which makes each galaxy fully unscreened is given in top right side of each panel. We ignore the possible radial dependence of fifth force while estimating the prediction. The vertical green lines show the bulge scale radius, below which we ignore the rotation measurements from the analysis and for fitting the density profile. In all but the lower right panel, the black and red curves show the fitted cSIS profiles for the stellar and gaseous rotation curves, respectively. The lower right panel shows the fitted NFW profile. It can be seen that the fitted values for the gaseous and stellar rotation curves differ slightly due to the fact that there are only a few points for the stellar curves, all of which are at very small distances from the galactic center. $v_{\rm max}$ is the maximum measured rotation velocities for the stellar and gaseous components, respectively. We also show the fitted values of r_0 and ρ_0 for the relevant profiles (cSIS for the first five panels and NFW for the lower right) for the stellar and gaseous rotation curves, respectively. Details of the analysis can be found in the text.

predict that $\Delta G/G > 0$ for the gaseous component and so cannot explain any observations of stars rotating faster than the gas. Additionally, $f(R)$ theory cannot explain a faster gaseous rotation than the predicted values given in Table IV.[5] Below, we comment on individual galaxies. The list is ordered in such a way that the first galaxy probes the smallest value of f_{R0} and last probes the largest. Also, we use the rejection sigma estimated after including astrophysical scatter for the following discussion. Here, we concentrate on $f(R)$ theories in order to focus on a concrete model and extend the analysis to more general models below. The measured rotation curves for each galaxy are plotted in Fig. 1.

(1) *ESO 4880490:* Both GR and $f(R)$ theories agree with the measured values within 1σ. However, this galaxy is self screened for $f_{R0} < 2.34 \times 10^{-7}$ and conclusions about $f(R)$ theories are applicable only for theories with f_{R0} larger than this. The intrinsic scatter in the rotation curve, which is common to dwarf galaxies, and astrophysical scatter are the major limiting factors which prevents us from drawing a stronger conclusion. This galaxy posses a small exponential bulge.[6]

[5]More general chameleon models can due to the freedom in the additional parameter α.

[6]Exponential bulges are different from classical bulges. The latter, found in elliptical galaxies, follow de Vaucouleurs's light profile and are supported by random velocity. On the other hand, exponential bulges are commonly found in disk galaxies. They follow exponential light profiles and are supported mostly by rotation.

TABLE IV. The stellar and gaseous rotation velocities for each galaxy in our sample after correcting for systematics. $v_{\rm gas}$ and $v_{\rm star}$ are the rotation velocities of the gaseous and stellar components in the range outside the bulge component of the galaxy, respectively. $\delta_v = v_{\rm gas} - v_{\rm star}$ and $\delta_v^{\rm predicted}$ is the $f(R)$ prediction for this difference. All the velocities are in units of km/s. The first part of the error is statistical and the second part is the intrinsic scatter in the rotation curve. The third error in δ_v shows the astrophysical scatter and the value in the bracket shows the effective error including all three sources. The rejection σ is the confidence with which we can reject predictions from $f(R)$ gravity. The first part of this column shows the significance after including all sources of error in the analysis and the value in brackets shows the significance without including the astrophysical scatter. A negative (positive) rejection σ implies that stars rotate faster (slower) than the gas.

Galaxy	$v_{\rm gas}$	$v_{\rm star}$	δ_v	$\delta_v^{\rm predicted}$	Rejection σ
ESO 4880490	$56.12 \pm 2.77 \pm 1.93$	$55.34 \pm 5.37 \pm 6.04$	$0.79 \pm 6.04 \pm 6.34 \pm 5.85$ (10.36)	8.56	−0.8 (−0.9)
ESO 2060140	$88.11 \pm 1.65 \pm 3.59$	$65.39 \pm 2.39 \pm 6.54$	$22.72 \pm 2.91 \pm 7.46 \pm 8.56$ (9.50)	10.12	1.3 (1.6)
ESO 2340130	$113.94 \pm 1.87 \pm 1.69$	$123.64 \pm 2.24 \pm 1.63$	$-9.70 \pm 2.92 \pm 2.35 \pm 12.49$ (13.15)	19.13	−2.2 (−7.7)
ESO 4000370	$83.19 \pm 2.24 \pm 1.42$	$58.42 \pm 2.99 \pm 7.07$	$24.78 \pm 3.74 \pm 7.21 \pm 7.85$ (9.47)	9.04	1.7 (1.9)
ESO 1860550	$119.69 \pm 3.57 \pm 5.32$	$158.83 \pm 3.15 \pm 2.69$	$-39.14 \pm 4.76 \pm 5.96 \pm 14.31$ (15.81)	24.57	−4.0 (−8.4)
ESO 5340200	$271.91 \pm 3.65 \pm 2.82$	$236.40 \pm 4.56 \pm 6.15$	$35.51 \pm 5.84 \pm 6.77 \pm 28.40$ (29.58)	36.57	0.0 (−0.1)

(2) *ESO 2060140:* $f(R)$ gravity agrees with the measurements more than GR. From table II it can be seen that this galaxy becomes self screened for $f_{R0} < 7.39 \times 10^{-7}$. This galaxy is a pure disk system with B/T = 0.04, which makes the galaxy a good candidate for testing modified gravity.

(3) *ESO 2340130:* This galaxy rejects $f(R)$ theories with $\sim 2\sigma$ and agrees with GR. This galaxy is screened by environment for $f_{R0} < 1.3 \times 10^{-6}$.

(4) *ESO 4000370:* This galaxy agrees with the $f(R)$ prediction (within $\sim 1\sigma$) better than the GR prediction (which is $> 2\sigma$ away). This galaxy is self screened for $f_{R0} < 2.77 \times 10^{-6}$ and therefore, the rejection is applicable only to models with f_{R0} larger than this.

(5) *ESO 1860550:* This galaxy rejects $f(R)$ with more than 3σ confidence. This galaxy is self screened for $f_{R0} < 1.49 \times 10^{-6}$. As described in Sec. V, removing more measured points from the inner part of rotation curves strengthen the significance of rejection.

(6) *ESO 5340200:* This galaxy agrees with the predictions of $f(R)$ and GR within 1σ but may not be able to constrain theories with $f_{R0} < 1 \times 10^{-6}$ due to self-screening.

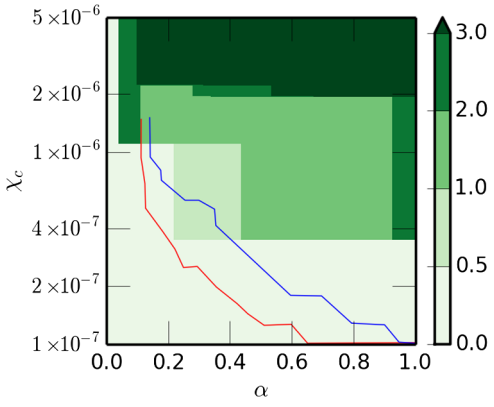

FIG. 2. Green contours show the limits obtained on the two parameters (χ_c and α) of chameleon theories. We show contours of 0.5σ, 1σ, 2σ, 3σ, where σ represents the confidence with which the corresponding parameter values can be rejected. We also show the 1σ and 2σ contours from [15]. It can be seen that the previous study give better constraints for $\alpha > 0.1$. This work is able to give upper limits on f_{R0} value for $\alpha < 0.1$.

It is important to note that the different screening levels of each galaxy mandate that we consider each separately when calculating the confidence with which we can reject modified gravity. This is not the case with GR since the equivalence principle is obeyed. In this case, one should take the average over all six galaxies and so the rejection σ for GR stated above should be taken equivocally; they are for comparison purposes only. Averaging over all six galaxies, we find $\langle \delta_v / v \rangle = 0.07 \pm 0.13$ and so the data are perfectly consistent with GR. A larger sample of unscreened galaxies would allow us to perform a similar analysis for modified gravity; such a comparison is meaningless for our current sample. It is also interesting to note that the galaxies ESO 2060140 and ESO 4000370 have similar rotation velocities and show a similar trend in the stellar and gaseous rotation curves.

Having elucidated the galaxies varying degrees of usefulness for probing modified gravity, we extend the analysis to general chameleon models to constrain the parameters χ_c and α. We consider α values between 0.05 and 1. Within this range, the Compton wavelength does not vary more than a factor of a few compared with the value at $\alpha = 1/3$[7] Figure 2 shows the combined constraints obtained for α and χ_c values using all the six galaxies. We show contours of 0.5σ, 1σ, 2σ, 3σ where σ represents the confidence with which we can reject the corresponding parameter range. We also show the previous constraints obtained by [15]. It can be seen that the constraints obtained from Cepheid observations are stronger compared to this

[7]This is important for addressing the environmental screening status of the galaxies, which is calibrated on $f(R)$ models [31].

analysis, especially for $\alpha > 0.1$. For values of $\alpha < 0.1$ we find that rotation curves give a better upper bound on χ_c.

VII. SUMMARY

Chameleon theories of gravity predict large differences between the stellar and gaseous rotation curves of isolated dwarf galaxies. Since stars are screened, they are expected to move according to GR whilst the unscreened gaseous component is predicted to rotate with a larger velocity. In this paper, we have used this effect to constrain the model parameters using observations of the rotation curves of six low mass galaxies.

The main results are summarized in Fig. 2, where we show the upper limits on the parameters, χ_c and α. For $f(R)$ theory, i.e., when $\alpha = 1/3$, we found that $f_{R0} > 1.5 \times 10^{-6}$ can be ruled out with more than 3σ confidence. For a general chameleon theory $\chi_c > 10^{-6}$ can be ruled out with 95% confidence down to $\alpha \approx 0.05$. This is a new and strong result, and it arises because the measured difference in velocity has the opposite sign from the chameleon predictions for some of the galaxies. This region of parameter space was previously unexplored due to the small signals predicted when $\alpha \ll 1$.

Other studies have constrained chameleon theories as well and here we discuss how our new constraints compare with previous bounds obtained using astrophysical tests.[8] [17] attempt to constrain $f(R)$ gravity based on several morphological and kinematical signatures using dwarf galaxies. Some of those tests indicate that $f_{R0} < 4 \times 10^{-7}$ but they show that better data are required to get significant constraints on the model parameters. Studies based on distance indicators [15] were able to rule out $f_{R0} > 4 \times 10^{-7}$ with more than 95% confidence. Our constraints at low α are an improvement over these constraints but at larger values the Cepheid bounds are stronger. It is worth noting that the novel features that arise in Cepheids, which are partially screened, are due to the increase in the strength of gravity and so they are not sensitive to small values of α. The test described here works when the galaxy is fully unscreened which is why we are able to probe into the regime $\alpha \lesssim 0.2$. Given that these are the early stages of testing modified gravity, it is valuable to use many different probes that rely on different physical systems, such as pulsating stars and disk galaxies.

As shown in Table IV, the astrophysical scatter in the rotation curve is one of the major limiting factors in this study. Such statistical uncertainties can be reduced by combining observations of several galaxies. For example, it can be seen that galaxies such as ESO 4880490 probe f_{R0} down to 2×10^{-7} but there is a large statistical uncertainty associated with the measurement. Based on the measured uncertainty, it can be seen that ≈25 similar low mass galaxies are enough to rule out $f_{R0} = 2 \times 10^{-7}$ with more than 4σ confidence. Future targeted observations of high signal-to-noise stellar rotation curves of isolated dwarf systems in the local Universe may serve that purpose.

One of the major assumptions in the above forecast is that the observed rotation velocity curves are free from systematics. Therefore, proper corrections for systematics such as asymmetric drift and nonrotational velocities are needed. Finally, it should be noted that several independent constraints on $f(R)$ parameters exist in the literature based on cosmological and lab experiments [40,52]. In this paper we limit our discussion only to astrophysical tests, which are emerging as a novel way of testing gravity.

[8] See [18,29,52] for a review of astrophysical tests.

ACKNOWLEDGMENTS

We are grateful to Bhuvnesh Jain for in-depth discussions and helpful suggestions. We thank Matthew Walker for many helpful suggestions. This work benefited from discussions with Lasha Berezhiani, Cullen Blake, Yi-Zen Chu, Joseph Clampitt, Mike Jarvis, Justin Khoury, Kazuya Koyama, Baojiu Li, Adam Lidz, Claudia Maraston, Alan Meert, Fabian Schmidt and Mitchell Struble. J. S. is supported by funds provided to the Center for Particle Cosmology by the University of Pennsylvania. Research at Perimeter Institute is supported by the Government of Canada through Industry Canada and by the Province of Ontario through the Ministry of Economic Development and Innovation.

[1] T. Clifton, P. G. Ferreira, A. Padilla, and C. Skordis, Phys. Rep. **513**, 1 (2012).
[2] K. Koyama, Rep. Prog. Phys. **79**, 046902 (2016).
[3] C. Burrage and J. Sakstein, J. Cosmol. Astropart. Phys. 11 (2016) 045.
[4] C. Burrage and J. Sakstein, Living Rev. Relativity **21**, 1 (2018).
[5] A. Vainshtein, Phys. Lett. B **39**, 393 (1972).
[6] J. Khoury and A. Weltman, Phys. Rev. D **69**, 044026 (2004).
[7] J. Khoury and A. Weltman, Phys. Rev. Lett. **93**, 171104 (2004).
[8] K. Hinterbichler and J. Khoury, Phys. Rev. Lett. **104**, 231301 (2010).

[9] P. Brax, C. van de Bruck, A.-C. Davis, and D. Shaw, Phys. Rev. D **82**, 063519 (2010).
[10] L. Hui, A. Nicolis, and C. W. Stubbs, Phys. Rev. D **80**, 104002 (2009).
[11] P. Chang and L. Hui, Astrophys. J. **732**, 25 (2011).
[12] B. Jain, R. Soc. London Phil. Trans. Series A **369**, 5081 (2011).
[13] B. Jain and J. Vanderplas, J. Cosmol. Astropart. Phys. 10 (2011) 032.
[14] A.-C. Davis, E. A. Lim, J. Sakstein, and D. Shaw, Phys. Rev. D **85**, 123006 (2012).
[15] B. Jain, V. Vikram, and J. Sakstein, Astrophys. J. **779**, 39 (2013).
[16] L. Hui and A. Nicolis, Phys. Rev. Lett. **109**, 051304 (2012).
[17] V. Vikram, A. Cabre, B. Jain, and J. VanderPlas, J. Cosmol. Astropart. Phys. 08 (2013) 020.
[18] J. Sakstein, Phys. Rev. D **88**, 124013 (2013).
[19] A. Terukina, L. Lombriser, K. Yamamoto, D. Bacon, K. Koyama, and R. C. Nichol, J. Cosmol. Astropart. Phys. 04 (2014) 013.
[20] H. Wilcox *et al.*, Mon. Not. R. Astron. Soc. **452**, 1171 (2015).
[21] J. Sakstein, Astrophysical tests of modified gravity, Ph.D. thesis, Cambridge University, 2014.
[22] K. Koyama and J. Sakstein, Phys. Rev. D **91**, 124066 (2015).
[23] J. Sakstein, Phys. Rev. Lett. **115**, 201101 (2015).
[24] J. Sakstein, Phys. Rev. D **92**, 124045 (2015).
[25] J. Sakstein, B. Jain, J. S. Heyl, and L. Hui, Astron. J. **844**, L14 (2017).
[26] J. Sakstein, Phys. Rev. D **97**, 064028 (2018).
[27] J. Sakstein and B. Jain, Phys. Rev. Lett. **119**, 251303 (2017).
[28] B. Jain and J. Khoury, Ann. Phys. (Amsterdam) **325**, 1479 (2010).
[29] A. Joyce, B. Jain, J. Khoury, and M. Trodden, Phys. Rep. **568**, 1 (2015).
[30] L. Lombriser, Ann. Phys. (Amsterdam) **526**, 259 (2014).
[31] A. Cabre, V. Vikram, G.-B. Zhao, B. Jain, and K. Koyama, J. Cosmol. Astropart. Phys. 07 (2012) 034.
[32] A. Pizzella, E. M. Corsini, M. Sarzi, J. Magorrian, J. Méndez-Abreu, L. Coccato, L. Morelli, and F. Bertola, Mon. Not. R. Astron. Soc. **387**, 1099 (2008).
[33] P. Brax, C. van de Bruck, A.-C. Davis, and D. J. Shaw, Phys. Rev. D **78**, 104021 (2008).
[34] W. Hu and I. Sawicki, Phys. Rev. D **76**, 064004 (2007).
[35] B. Li and G. Efstathiou, Mon. Not. R. Astron. Soc. **421**, 1431 (2012).
[36] F. Schmidt, A. Vikhlinin, and W. Hu, Phys. Rev. D **80**, 083505 (2009).
[37] G.-B. Zhao, B. Li, and K. Koyama, Phys. Rev. D **83**, 044007 (2011).
[38] G.-B. Zhao, B. Li, and K. Koyama, Phys. Rev. Lett. **107**, 071303 (2011).
[39] W. J. G. de Blok, Adv. Astron. **2010**, 1789293 (2010).
[40] L. Lombriser, F. Schmidt, T. Baldauf, R. Mandelbaum, U. Seljak, and R. E. Smith, Phys. Rev. D **85**, 102001 (2012).
[41] B. Li, W. A. Hellwing, K. Koyama, G.-B. Zhao, E. Jennings, and C. M. Baugh, Mon. Not. R. Astron. Soc. **428**, 743 (2013).
[42] H. Desmond, P. G. Ferreira, G. Lavaux, and J. Jasche, Mon. Not. R. Astron. Soc. **474**, 3152 (2018).
[43] H. Desmond, P. G. Ferreira, G. Lavaux, and J. Jasche, arXiv:1802.07206.
[44] A. Boselli, *A Panchromatic View of Galaxies* (Wiley, New York, 2012).
[45] C. Conroy, Annu. Rev. Astron. Astrophys. **51**, 393 (2013).
[46] S.-H. Oh, W. J. G. de Blok, F. Walter, E. Brinks, and R. C. Kennicutt, Jr., Astron. J. **136**, 2761 (2008).
[47] C. Trachternach, W. J. G. de Blok, F. Walter, E. Brinks, and R. C. Kennicutt, Jr., Astron. J. **136**, 2720 (2008).
[48] J. Binney and S. Tremaine, *Galactic Dynamics*, 2nd ed. (Princeton University Press, Princeton, NJ, 2008).
[49] J. L. Hinz, H.-W. Rix, and G. M. Bernstein, Astron. J. **121**, 683 (2001).
[50] K. A. Oman *et al.*, Mon. Not. R. Astron. Soc. **452**, 3650 (2015).
[51] W. A. Hellwing, C. S. Frenk, M. Cautun, S. Bose, J. Helly, A. Jenkins, T. Sawala, and M. Cytowski, Mon. Not. R. Astron. Soc. **457**, 3492 (2016).
[52] B. Jain, A. Joyce, R. Thompson, A. Upadhye *et al.*, arXiv: 1309.5389.